PHYSICS OF PARTICLE ENTRAINMENT UNDER THE INFLUENCE OF AN IMPINGING JET

Robert Haehnel
U.S. Army Engineer Research and Development Center
Cold Regions Research and Engineering Laboratory
Hanover, NH 03755

W. Brian Dade
Dartmouth College
Hanover, NH 03755

ABSTRACT

In the laboratory we used an idealized rotorwash flow—an axisymmetric jet impinges normally on a packed bed of cohesionless particles—and measured the spatially varying flow field and entrainment flux under an axisymmetric jet over a range of jet exit velocities and bed materials. We found that the erosion of the bed is driven by turbulent surface shear stress, quantified by the turbulent kinetic energy of the flow. This observation differs from uniform flow parallel to the bed wherein the flux of particles being removed from the bed depends linearly on the average surface shear stress of the fluid imposed on the bed. We discuss the implications of these findings for applying a general model for capturing particle entrainment under impinging flows.

1. INTRODUCTION

Brownout occurs during rotorcraft operations (e.g. landing, takeoff, sling load operations) over dry loose soils. This may eliminate all visual cues for the pilot leading to loss of situational awareness, collisions with other aircraft or ground based objects, damage to equipment and loss of life. A virtual simulation capability of the brownout environment would allow simulation of dust cloud evolution in complicated flow conditions such as a helicopter rotorwash impinging on sand or dust covered ground. Algorithms exist to model all of the processes governing brownout cloud evolution except for the appropriate entrainment (particle pick-up) boundary condition for the particle transport equation.

Physics of particle entrainment from a packed bed due to an impinging turbulent jet (e.g. Fig. 1) has received limited attention; yet, particle exchange at the bed is the boundary condition for the governing particle transport equation

$$\frac{\partial c}{\partial t}+\frac{\partial uc}{\partial x}+\frac{\partial vc}{\partial y}+\frac{\partial (w-w_f)c}{\partial z}= D\left(\frac{\partial^2 c}{\partial x^2}+\frac{\partial^2 c}{\partial y^2}+\frac{\partial^2 c}{\partial z^2}\right)-\frac{\partial}{\partial x}\overline{c'u'}-\frac{\partial}{\partial y}\overline{c'v'}-\frac{\partial}{\partial z}\overline{c'w'} \quad (1)$$

where u, v, w are the velocity components in the x, y and z directions, c is the particulate concentration, and D is the diffusion coefficient. Gravitational effects are taken into account using w_f, the particle fall velocity. The primed terms are fluctuating components of velocity and concentration, and the overbar indicates an average value. Equation (1) is often referred to as the scalar transport equation written in Reynolds Average form. The terms $\overline{c'u'}$, $\overline{c'v'}$ and $\overline{c'w'}$ are called the Reynolds sediment fluxes. The entrainment from the bed into the flow is governed by $Q_s=\overline{c'w'}\big|_{z=0}$, which is provided as a boundary condition via a suitable "entrainment function." For the present we consider $\overline{c'u'}=\overline{c'v'}=0$ at the bed surface. Once an appropriate entrainment function is identified for a flow of interest (1) can be readily solved numerically in standard computational fluid dynamics (CFD) codes, when coupled with continuity, momentum and energy equations. The challenge arises in choosing the correct entrainment function for the flow of interest. For the non-uniform flow of an impinging jet an appropriate entrainment function has not yet been developed; without this boundary condition accurate numerical simulation of dust and snow cloud formation due to helicopter downwash is not possible.

A reasonable starting point in developing a predictive model of an impinging jet would be to use existing entrainment functions and apply them to the impinging jet problem using (1). Two flows for which entrainment functions have been developed are fluidized bed flow and uniform steady parallel flow (USPF).

Aspects of both of these flows are present in an impinging jet. Though concepts can be borrowed from the body of knowledge available for both fluidized beds and parallel flows it cannot be assumed that the entrainment functions developed for these flow regimes can be used in non-uniform flows and further understanding of the flow characteristics and entrainment processes under the influence of an impinging turbulent jet is required.

Report Documentation Page

Form Approved
OMB No. 0704-0188

1. REPORT DATE	2. REPORT TYPE	3. DATES COVERED
DEC 2008	**N/A**	**-**

4. TITLE AND SUBTITLE	5a. CONTRACT NUMBER
Physics Of Particle Entrainment Under The Influence Of An Impinging Jet	5b. GRANT NUMBER
	5c. PROGRAM ELEMENT NUMBER
6. AUTHOR(S)	5d. PROJECT NUMBER
	5e. TASK NUMBER
	5f. WORK UNIT NUMBER
7. PERFORMING ORGANIZATION NAME(S) AND ADDRESS(ES) **U.S. Army Engineer Research and Development Center Cold Regions Research and Engineering Laboratory Hanover, NH 03755**	8. PERFORMING ORGANIZATION REPORT NUMBER
9. SPONSORING/MONITORING AGENCY NAME(S) AND ADDRESS(ES)	10. SPONSOR/MONITOR'S ACRONYM(S)
	11. SPONSOR/MONITOR'S REPORT NUMBER(S)

12. DISTRIBUTION/AVAILABILITY STATEMENT
Approved for public release, distribution unlimited

13. SUPPLEMENTARY NOTES
See also ADM002187. Proceedings of the Army Science Conference (26th) Held in Orlando, Florida on 1-4 December 2008, The original document contains color images.

14. ABSTRACT

15. SUBJECT TERMS

16. SECURITY CLASSIFICATION OF:			17. LIMITATION OF ABSTRACT	18. NUMBER OF PAGES	19a. NAME OF RESPONSIBLE PERSON
a. REPORT	b. ABSTRACT	c. THIS PAGE			
unclassified	**unclassified**	**unclassified**	**UU**	**8**	

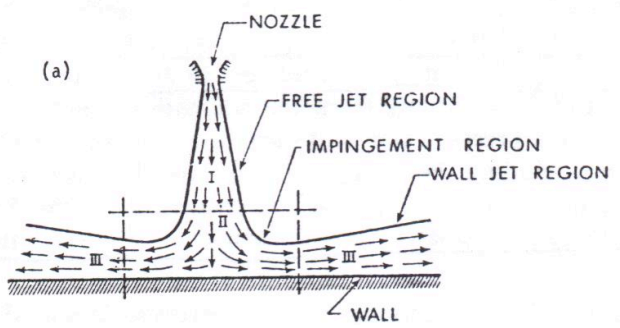

Figure 1. Geometry of the flow from a jet impinging normal to a flat particle bed. Region I is the free jet region where the flow is not influenced by the presence of the wall. Region II is the impingement zone where the flow stagnates and turns to the follow the bed. In Region III the flow can be characterized as a radially expanding wall jet and the flow is predominately parallel to the bed (Beltaos and Rajaratnam 1974).

A related area of research is scour hole or crater formation caused by an axisymmetric jet impinging on a packed bed. However, in this area of research emphasis has been on the geometry of the scour hole or crater (e.g. *Rajaratnam & Beltaos* 1977, *Kobus et al.* 1979, *Rajaratnam* 1982, *Aderibigbe & Rajaratnam* 1996, *Gioia & Bombardelli* 2005, *Bombardelli & Gioia* 2006, *Haehnel et al.* 2006, 2008) or the average shear stress acting on the bed surface (*Poreh et al.* 1967, *Beltaos & Rajaratnam* 1974, 1977, *Phares et al.* 2000, *Rajaratnam & Mazurek* 2005) rather than the entrainment physics.

The objective of this work is to study in the laboratory particle entrainment physics under an impinging flow striking a particle bed, and the associated turbulent flow field. From these efforts we develop an entrainment boundary condition appropriate for use in modeling unsteady impinging flows such as rotorcraft-induced brownout. In the laboratory we measured the erosion rate of the packed bed and relate this to the turbulent shear stress acting on the bed and found that the Reynolds stress acting on the bed is the driving force for entraining the particles from the bed into the flow. This allows us to pose a generalized entrainment function (or boundary condition) applicable for uniform and non-uniform flows. This has potential application to describing sedimentation processes in expanding channels as well as impinging jets.

2. EXPERIMENTAL APPROACH

The experiments were conducted in two parts, (1) document the erosion rate for particles being removed from the packed bed due to an impinging jet and (2) measure the turbulent flow field over the packed bed. These two sets of experiments are described in turn.

Figure 2a shows the experimental set up for the erosion experiments. A particle bed is place on the floor of the test chamber. The bed is 2.44m × 2.44m × 3.81cm deep; two particle types were used, spherical glass beads and Ottawa sand. The properties of these particles are given in Table 1. At the top of the chamber a 0.77 cm diameter nozzle was mounted 118.7 cm above the bed. This nozzle height was chosen to create an erosion pattern in the bed that was on the order of 1 m in diameter, making it easy to measure the spatial variation in erosion flux using a surface profilometer. The exit velocity of the nozzle was varied from approximately 140 to 250 m/s. A compressor delivering 100 – 120 psi pressure supplied the air. The velocity exiting the nozzle was controlled using a feedback loop between an EPI Mastertouch™ flow meter mounted in the airline and a Mesto Automation™ pneumatic control valve. The exit velocity was maintained to within 1.5 % over the duration of each experiment.

The radially varying volumetric erosion rate of the bed was measured by using an Omron™ ZS-LD350S laser range finder mounted on a three-axis traversing system suspended from the top of the test chamber (the measurement accuracy of the laser range finder was typically better then ± 0.5 mm). The initial surface profile of the flat bed surface was measured with this laser profiler. The jet was then run for a short period of time, Δt (e.g. 15 – 30 seconds, depending on the jet exit velocity) and the erosion pattern was then measured with the laser profiler. A typical scour pattern is shown in Figure 2b and a measured surface profile is shown in Figure 2c. The erosion rate, E, was then computed by taking the difference in the two profiles, Δh, and for each grid point, i, in the profile: $E_i = \Delta h_i / \Delta t$. This gives the net average erosion rate for each grid point. This was done for four jet exit velocities: 140, 165, 190, 250 m/s nominally. For the erosion rate experiments two repetitions were obtained at each of the target velocities. For the sand, only the three highest jet exit velocities were used because there was no material removed during the test with the lowest velocity: 140m/s.

The second set of tests document the shear stress on the bed surface. Fundamentally, the bed (or wall) shear stress, τ_w, is proportional to the velocity gradient at the wall (Newton's law of viscosity applied at the wall)

$$\tau_w = \rho \nu \left. \frac{du}{dz} \right|_w \qquad (2)$$

Table 1. Properties of the particles used in this study.

	Mean diameter, d_s (μm)	Particle density, ρ_s (kg/m^3)	Effective Roughness*, k_s' (mm)	Angle of repose (deg)	Shape
Glass beads	134	2440	1.1	21.3	Spherical
Ottawa Sand	560	2600	3.0	33	Angular

* The values of k_s' reported are for $R_s > 100$ (fully rough flow).

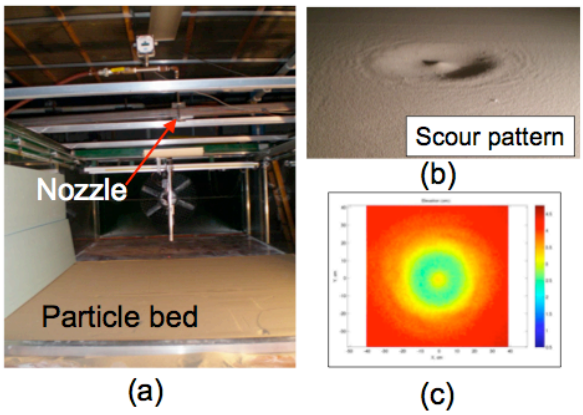

Figure 2. Test set up for erosion experiments. (a) A particle bed is placed on the floor of the chamber and a nozzle is on the ceiling of the chamber. (b) Shows the scour pattern that results in the particle bed after the jet has been run for a short time; (c) is a typical surface profile measured for the scour pattern.

where ρ and ν is the fluid density and kinematic viscosity. Ideally, we want to measure the shear stress over the actual erodible bed as the material is being removed from the bed. In principle this can be done using a velocity probe and measure the velocity gradient over the surface. The problem with this approach is that the bed is continuously receding under the probe as the measurement is being taken; therefore the elevation is continuously changing as we are trying to measure the velocity at a fixed elevation above the bed. A different approach was needed.

Nikuradse (1933) found the velocity profile $u(z)$ over a rough bed can be expressed as

$$u(z) = \frac{u_*}{\kappa} \ln \frac{z}{k_s} + B(R_s) \qquad (3)$$

where u_* is the friction velocity ($u_* \equiv \sqrt{\tau / \rho}$), κ= 0.41, von Karman's constant, k_s is the effective bed roughness ($k_s \propto d_s$, particle diameter, but in general $ks \neq d_s$), and B is a function of $R_s = u_* k_s / \nu$. Thus, the velocity profile is a function of the bed shear stress (via u_*) and the effective bed roughness, k_s. Suspended sediment modifies the velocity profile over the bed due to the mobile particles removing energy from the fluid flow. Therefore the effective roughness for a mobile bed, k_s', is larger than that measured over a static bed, k_s containing the same sized particles. This results in a modified shear stress in comparison to that over a static bed. Therefore, by analogy we can determine k_s' for the mobile bed and then create a static bed that has $k_s = k_s$' and measure the shear stress over the static bed to get an estimate of the shear stress associated with erosion over a bed with particles in motion.

We followed this later approach to determine the shear stress over an erodible bed. To do this we had to measure of k_s' for the mobile bed. This was determined by putting the bed material on the floor of the CRREL Snow Drift Wind Tunnel (*Anno* 1987, *Haehnel et al.* 1993), measuring the velocity profile over the bed while the particles were in motion an then using eq. (3) to determine k_s'. Table 1 provides the values of k_s' determined for the particles used in this study. Once k_s' was determined for the glass beads and sand, surfaces were prepared that had a $k_s = k_s$' so that the velocity profile near the surface for these static beds matched very closely that over the erodible beds used to measure the erosion rate in the first set of experiments.

The shear stress over these static beds was determined using two instruments, a hot film anemometer (HFA) and pitot-static tube (pitot), and four methods as follows:

1. Log profile: We measured the time averaged vertical velocity profile over the bed, and fit a log-law to the data in the boundary layer portion of the radially expanding wall jet. Then the shear stress is determined from $\tau_w = \rho u_*^2$ and eq. (3).
2. Preston method (or Preston): We measured the time averaged velocity very close to the surface and assume a log-law profile, of the form proposed by Nikuradse (1933) (eq. 3), between that height and the effective roughness height, k_s. This method was first proposed by *Preston* (1954) for measuring the shear stress on a smooth surface. It was adapted for measuring the shear stress on a rough surface by *Hollingshead & Rajaratnam* (1980).
3. Turbulent shear ($\overline{v'w'}$): We extrapolate the measured Reynolds shear stress, $\overline{v'w'}$, to the ground plane (*Pope* 2000). This extrapolated value is equal to the wall shear stress: $\tau_w' = \tau_w / \rho = \overline{v'w'}\big|_{\to w}$.

4. Turbulent Kinetic Energy (TKE): Use the relationship $\overline{v'w'} = 0.2\text{TKE}$ where TKE = ½ ($u'^2+v'^2+w'^2$). Like method 3 we extrapolate TKE to the ground plane as well. This method is used to estimate the Reynolds stress based on the turbulent fluctuations of each component, rather than the average of the product of the turbulent components. Though it is desirable to obtain the Reynolds stress directly (method 3), this is difficult to do in practice. If the anemometer probe used to measure the velocity field is not precisely aligned with the flow, v' can be contaminated by w' and vice versa leading to poor resolution of the Reynolds stress field. TKE correlations to the Reynolds stress are not prone to the problems of probe misalignment and therefore it is easier to accurately measure the Reynolds stress by this technique.

For all of these methods data was taken for 64s. The sample rate for the HFA data was 2kHz, while for the pitot tube the sample rate was 200 Hz. Methods 1 & 2 used temporal averages (first moments u, v & w) of both the HFA and pitot tube data. Methods 3 and 4 used the second moments of the velocity data, u', v' & w' computed from the HFA data only. Two velocity profiles were taken at each of the target jet velocities in this set of experiments, one with each instrument type.

3. RESULTS AND DISCUSSION

Figure 3 shows sample erosion rate measurements. Figure 3a gives the erosion rate based on the first surface profile measured for that experiment. The solid line is an average of the data along four sections taken starting at the jet centerline and extending out in the positive and negative directions along the x and y-axes. The dashed lines indicate the range in the measured erosion rate. Figure 3b shows the erosion rate for each of the four successive profiles taken during this test. It is noted that only the first profile started with a flat surface. The successive profiles were a continuation of the test and started with the surface relief obtained at the end of the previous time step. The erosion rate was determined for each of these following measurements by using the change in height between successive profiles. Regardless, even though the initial conditions for profiles 2 and beyond was not a flat surface Figure 3b shows that there was very little difference in the average erosion rate measured. Thus, for the minimal surface relief observed in these experiments (≤ 3.81cm) there was no profound difference in the erosion rate. Similar results were observed for all of the other tests using both sand and glass beads.

Figure 4 shows comparisons of all of the stress measurements for the k_s' = 1.1 mm (associated with glass beads). Similar results were obtained for k_s' = 3 mm (sand). In this and flowing figures we use a reduced shear stress, $\tau_w' = \tau_w/\rho = u_*^2$. We will use reduced shear stress and shear stress interchangeably throughout the remainder of this work.

The four plots in Figure 4 show several things. First, all four methods give a shear stress that is generally within the same order of magnitude for methods 2-4. The shear stress measured with method 1 is much lower. Second, there is good agreement between the data taken using the HFA and pitot tube showing consistent results for both methods.

Now we will consider each stress measure in turn. Though we have obtained very good results estimating the shear stress from the log profile with uniform parallel flow in the wind tunnel, where the thickness of the boundary layer is 10 - 20 cm, this method does not seem to work well for the thin boundary layer under an impinging jet. The velocity profile of the radially expanding flow is essentially a wall jet, which has a velocity profile that increases in the vertical, reaches a peak and then declines as height continues to increase. In these experiments we measured the velocity every 0.5 mm between 2 mm and 12 mm above the bed with the HFA and 1.5 to 11.5 mm for the pitot tube (because the pitot tube was thinner in diameter we could measure the velocity closer to the surface with that instrument). The height at which the peak velocity in the wall jet occurred was generally less than 12 mm, except at large radial distances from the jet centerline (radius, r > about 35cm, r/H > about 0.3). The thickness of the log-law boundary layer (BL) was even thinner than that. We digitized the height of the top of the log-law region for each of the velocity profiles and found that near the jet centerline the BL was on the order of 2 mm or less. Thus, for small r/H there were not sufficient points to resolve the log profile for r/H less than about 0.05. So we cannot use this method in this region. Above r/H ≈ 0.1 there are enough points to get a fit to the data and get an estimate for the shear stress using this method, though the predicted shear stress is very noisy and is much smaller than the shear stress determined by the other methods.

Rajaratnam & Mazurek (2005) had similar problems trying to determine the wall shear stress from the log profile under an impinging jet, and disbanded using that method because the results were too noisy. Thus, they adopted a different method to measure the friction velocity; they used a Preston tube as described above. This method was originally developed by *Preston* (1933) to measure the shear stress over an airfoil where the BL is very thin. We used the data we obtained from both instruments to calculate the shear stress by this method using the procedures outlined by *Hollingshead & Rajaratnam* (1980) and *Wu & Rajaratnam* (2000).

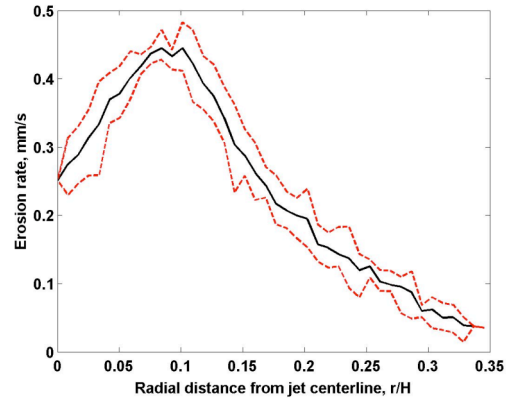

(a)

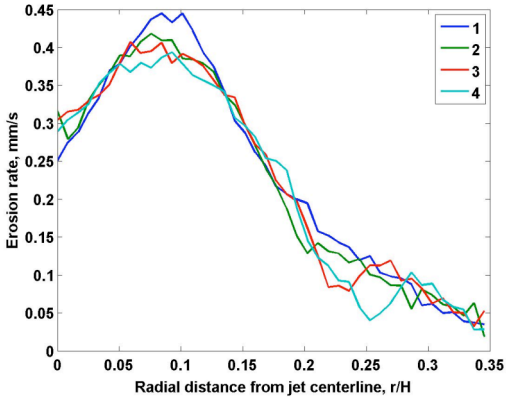

(b)

Figure 3. Representative erosion rate measurements for glass bead experiments (jet exit velocity is 247 m/s). The erosion rate for the first profile is shown in (a). The average flux is indicated by the solid line, the range in data is indicated by the dashed line. All four profiles for that experiment are shown in (b). Δt = 19 s for this test.

The shear stress computed this way gives a very noise free result that agrees well in magnitude with methods 3 and 4. The general trend shown for this measure of the shear stress is the average τ_w' is zero at the jet centerline and then peaks at about r/H = 0.13 – 0.16 and then declines in the radial direction. The shear stress determined by methods 3 and 4 shows a similar overall trend to that of method 2, but there are noticeable differences. First, the shear stress does not go to zero at the jet centerline. Second, the location of the peak shear stress for these two methods occurs closer to the jet centerline (r/H < 0.1), approximately the same location where the peak erosion rate is observed (see Fig. 3).

The shear stress determined using method 2 (Preston tube) is based on the long term temporal average of the velocity, which does on average go to zero at the jet center line (i.e. the jet stagnation point). Though the temporal average of the velocity may go to zero, due to turbulent fluctuations in the flow the instantaneous velocity may not be zero at any given time. This is borne out by the measures of shear stress using methods 3 and 4 that are based on the fluctuating components of the velocity field (Reynolds stress or turbulent shear stress). Though at the stagnation point the average shear stress (based on the average velocity: method 2) goes to zero, the shear stress based on the fluctuating components of the flow, v and w, does not go to zero.

It is generally accepted that methods 3 and 4 are alternate ways to determine the wall shear stress obtained in methods 1 and 2. For reasons previously mentioned, we discard the results obtained from method 1 in this study. Comparisons of the remaining methods show that near the jet centerline there is gross disagreement between method 2 (Preston tube) and methods 3 and 4 (Reynolds stress measures). Yet, at large radial distances (r/H > 0.25 – 0.3) there is good agreement between methods 2, 3 & 4. This suggests that for complicated flows, such as an impinging jet, this shear stress correlation breaks down. Yet, for large r/H the flow is more like USPF where the correlation is valid.

Conventional entrainment functions that apply to USPF (e.g. *Meyer-Peter & Muller* 1948, *Akiyama & Fukushima* 1986, *Garcia* 1989, *Pomeroy & Gray* 1990, *Cao* 1997, *Maticorena & Bergametti* 1995, *Maticorena et al.* 1997, *Liston & Sturm* 1998, *Draxler et al.* 2001, *Etoh & Fukushima* 2001, *Fukushima et al.* 2001, *Doorschot & Lehning* 2001, *Beyers et al.* 2004) characterize the entrainment flux, q, as a function of the mean shear stress (or friction velocity) acting on the particle bed: $q = f(\tau_w)$; we assume that $q \sim E$ also. If this holds true for an impinging jet, then the data should collapse on a single line if we plot E vs. τ_w as we have done in Figure 5. Yet, we find this is not the case. In Figure 5a we see that where the average shear stress is zero (i.e. the centerline of the jet) there is significant entrainment occurring. If the average shear stress drives entrainment then where the shear stress is zero the erosion rate should be zero also. This is clearly not the case for Figure 5a. Figure 5b shows a similar trend for the sand particles, though the trend is not as clear as for the glass beads.

The results shown in Figure 5 can be explained by considering the data plotted in Figure 4. Though the average shear stress is zero at the jet centerline, the shear stress based on the turbulent fluctuations of the flow (Reynolds stress) does not go to zero at the jet centerline. Generally the trend for both Reynolds stress measures ($\overline{v'w'}$ or 0.2TKE) is the same though the measure based on the TKE is less noisy. Therefore, we have chosen to use the measured Reynolds stress based on the TKE to characterize the spatially varying turbulent shear stress.

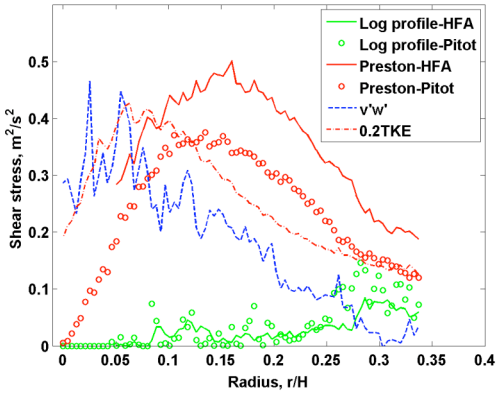

Figure 4. The radial varying shear stress determined by four different methods for an average jet exit velocity of 187m/s. The shear stress plotted is a reduced shear stress $\tau_w' = \tau_w/\rho = u_*^2$.

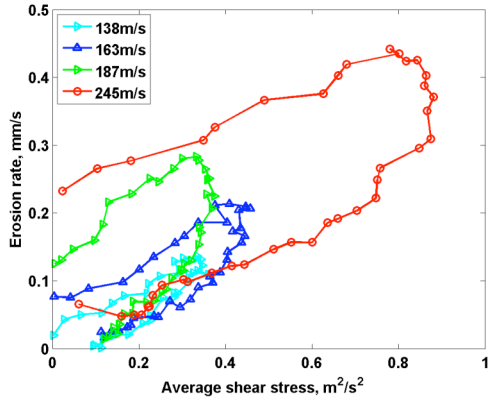

(a) Glass beads

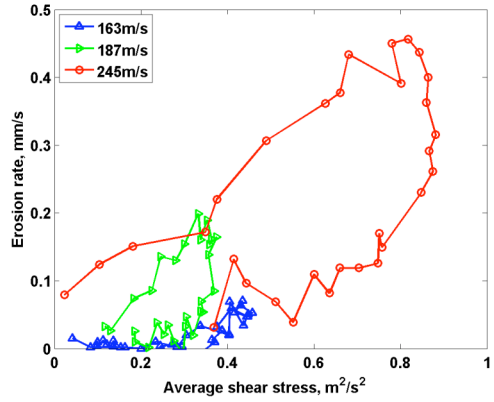

(b) Sand

Figure 5. Erosion rate as a function of average surface shear stress for (a) glass beads and (b) Ottawa sand. The legend indicates the jet exit velocity associate with each data set. The shear stress plotted is a reduced shear stress $\tau_w' = \tau_w/\rho = u_*^2$.

In Figure 6 we plot the erosion rate vs. Reynolds stress based on TKE. The results appear to indicate a threshold or critical shear stress, τ_c', of about 0.075 m^2/s^2 for the glass beads and 0.13 m^2/s^2 for the sand indicated by the rapid drop off in the entrainment rate at the left side of he curve. Above the threshold there is a nearly linear response in the data. This suggests that the Reynolds stress provides a more general collapse of the data than the average shear stress, though clearly the collapse is better for the glass beads than for the sand data.

The presence of this sharp critical entrainment condition in the data suggests the functional form for the entrainment flux proposed by *Pomeroy & Gray* 1990, *Maticorena & Bergametti* 1995, *Cao* 1997 and others

$$q = K / g(\tau_w - \tau_c) \qquad (4)$$

where g is the gravitational constant and K is a constant with units of m^{-1}. The solid line in Figure 6 is a plot of eq. (4) with $K = 7.7\ m^{-1}$.

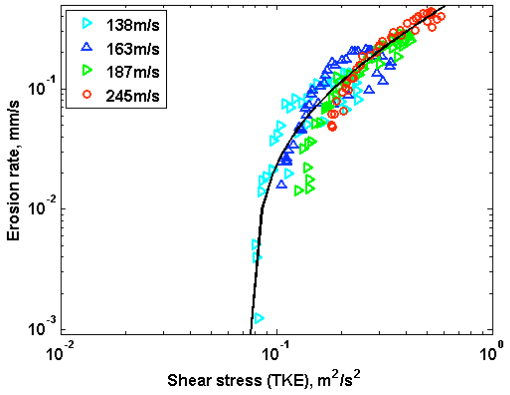

(a) Glass beads

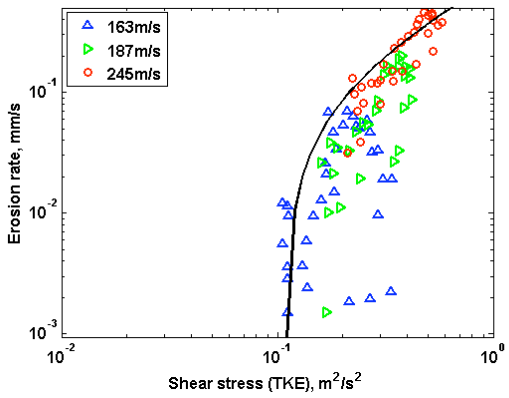

(b) Sand

Figure 6. Erosion rate for (a) Glass beads and (b) Ottawa sand as a function of the Reynolds stress computed from 0.2TKE. The solid line is a plot of eq. (4) with $\tau_c' = 0.075$ *and 0.13 for the glass beads and sand, respectively. The shear stress plotted is a reduced shear stress* $\tau_w' = \tau_w/\rho = u_*^2$.

The data we obtained for a jet impinging on a bed of particles suggests that the driving force for particle entrainment is a result of the Reynolds stress—which is associated with the turbulent fluctuations in the flow—acting on the bed. This of course is the same as the average shear stress in the case of USPF. However, we clearly show that for complicated flows such as an impinging jet there is little correlation between the shear stress based on the average flow (the first moment of the velocity field) and the Reynolds stress (based on the second moment of the velocity field). This suggests that eq. (4) has general applicability provided the shear stress is computed in general from the Reynolds stress extrapolated to the surface:

$$\tau_w = \rho \overline{v'w'}\Big|_{\to w} \qquad (5)$$

Because of the interchangeability of the shear stress based on the average flow field and that computed from the Reynolds stress (eq. 5) in uniform parallel flow the critical shear stress required for eq. (4) can be determined based on the empirical data and relationships put forward by *Shields* (1936) and *Yalin & Karahan* (1979), *Bagnold* (1941), *Iversen & White* (1982) and *Shao & Lu* (2000) and others. For example the expression put forward by *Shao & Lu* (2000)

$$\tau_c = A^2 \left(\Delta\rho g d_s + \frac{\beta}{d_s} \right) \qquad (6)$$

is simple and applicable to both aqueous and eolian flows. For aqueous flows $A = 0.2236$ and $\beta = 7.6\times10^{-5}$ N m^{-1}, while for eolian flows $A = 0.1109$ and $\beta = 3\times10^{-4}$ N/m. In eq. (6) $\Delta\rho = \rho_s - \rho$. Based on eq. (6) the estimated critical shear stress for the glass beads and sand are 0.059 and 0.15 m^2/s^2, respectively. This agrees well with the observed values obtained from Figure 6: 0.075 and 0.013 m^2/s^2 for glass and sand, respectively.

The forgoing suggests a conceptually simple methodology for applying an entrainment function to model the entrainment flux boundary condition under complex flow conditions such as an impinging jet. Conventional entrainment functions such as eq. (4) can be applied to a general flow condition provided the wall shear stress is determined using a turbulent stress measure obtained from the flow (e.g. methods 3, 4 or some other appropriate method). This requires the flow solver to accurately resolve the turbulent fluctuations of the flow. Particle cloud evolution can then be readily simulated using the scalar transport equation and conventional CFD techniques.

CONCLUSIONS

We measured the rate of entrainment of particles being removed from a particle bed under the influence of an impinging jet and the associated surface shear stress that drives particle entrainment. We found that the entrainment rate does not correlate well with the surface shear stress computed from the average flow (the first moment of the velocity field). However, there is very good correlation between the surface shear stress computed from the Reynolds stress, which is based on the turbulent fluctuations in the flow (the second moment of the velocity field). These results show that published expressions that quantify the entrainment flux for uniform flow that acts parallel to the surface can also be used as a particle flux boundary condition in complicated flow conditions, such as an impinging jet, provided the surface shear stress used in these equations be computed using methods that involve the turbulent fluctuations in the flow (e.g. the second moments of the velocity field). This requires that CFD methods accurately resolve the second moments in the velocity field in complicated fluid flows.

AKNOWLEDGEMENTS

This effort was funded by the Army In-house Laboratory Innovative Research (ILIR) program "Physics of particle entrainment under an impinging jet." The authors would like to thank Jesse Stanley who helped with set up and automation of the experiments.

REFERENCES

Aderibigbe, O.O. and N. Rajaratnam, 1996: Erosion of loose beds by submerged circular impinging vertical turbulent jets. *J. of Hyd. Res.*, **34**:1 19-33.

Akiyama, J. and Fukushima, Y., 1986: Entrainment of non-cohesive bed sediment into suspension, Third International Symposium on River Sedimentation, University of Mississippi, 31 Mar-4 Apr.

Anno, Y., 1987: "CRREL's Snowdrift wind tunnel." Proc. 3rd Cold Region Technology Conference, Sapporo, Japan, Nov.

Bagnold, R.A., 1941: *The Physics of Blown Sand and Desert Dunes*, Methuen, London.

Beltaos, S. and Rajaratnam, N., 1974: Impinging circular turbulent jets, *Journal Hydraulic Division*, ASCE **100**: 1313-1328.

Beyers, J.H.M., Sundsbo, P.A. and Harms, T.M., 2004: Numerical simulation of three-dimensional, transient snow drifting around a cube. Journal of wind engineering and Industrial Aerodynamics, **92**:9, July, pp. 725-747.

Bombardelli, F. A. and G. Gioia, 2006: Scouring of granular beds by jet-driven axisymmetric turbulent cauldrons, *Phy. Of Fluids*, **18**: 088101.

Cao, Zhixian, 1997: "Turbulent bursting-based sediment entrainment function." *J. of Hydraulic Engineering*, **123**:3, 233-236.

Doorschot, J.J.J. and M. Lehning, 2001: Equilibrium saltation: mass fluxes, aerodynamic entrainment and

dependence on grain properties. *Boundary-Layer Metrology* **104**: 111-130.

Draxler, R.R., Gillette, D.A., Kirkpatrick, J.S. and Heller, J., 2001: Estimating PM_{10} air concentrations from dust storms in Iraq, Kuwait and Saudi Arabia, *Atm. Env. 35*, 4315-4330.

Etoh, T. and Fukushima, Y., 2001: Numerical Analysis of Turbidity Currents using k-ε Turbulence model, 8th international Symposium on Flow Modeling and Turbulence Measurements (FMTM2001), IAHR.

Fukushima, Y., Etoh, T., Ishiguro, S., Kosugi, K. and Sato, T., 2001: Flow Analysis of developing snowdrifts using a k-ε turbulence model, SEPPYO, Journal of the Japanese Society of Snow and Ice, Vol. 63, No. 4 (in Japanese).

Garcia, M.H., 1989: Depositing and Eroding Sediment-Driven Flows: Turbidity Currents, Doctorate Thesis, University of Minnesota.

Gioia, G. and F. A. Bombardelli, 2005: Localized Turbulent Flows on Scouring Granular Beds, *Phy. Rev. Letters*, **95**: 0114501.

Haehnel, R.B., W.B. Dade, B. Cushman-Roisin, 2008: "Crater evolution due to a jet impinging on a bed of loose particles," 11th ASCE Earth & Space Conference, March 3-6, Long Beach, CA.

Haehnel, R., B. Cushman-Roisin and W.B. Dade, 2006: "Cratering by a subsonic jet impinging on a bed of loose particles," ASCE Earth & Space 2006, Proceedings 10th ASCE Aerospace Division International Conference on Engineering, Construction and Operations in Challenging Environments, Houston, TX, 5-8 March.

Haehnel, R.B., J.H. Wilkinson, J.H. Lever, 1993: Snowdrift modeling in the CRREL wind tunnel, *Proceedings of the 50th Eastern Snow Conference*, Quebec City, Quebec, June 8-10, 1993, pp. 139-147.

Hollingshead and Rajaratnam 1980: A calibrataion chart for the Preston tube, *J. Hydr. Res.* **18**:4.

Iversen, J.D., and White, B.R., 1982: Saltation Threshold on Earth, Mars and Venus, *Sedimentology*, **29** 111-119.

Kobus, H., P. Leister and B. Westrich, 1979: Flow field and scouring effects of steady and pulsating jets impinging on a movable bed. *J. of Hyd. Res.* **17**:3 175-192.

Liston, G.E. and M. Sturm, 1998: A snow-transport model for complex terrain, *J. of Glac.*, **44**:148, 498-516.

Marticorena, B. and Bergametti, G., 1995: Modeling the atmospheric dust cycle: 1. Design of a soil-derived dust emission scheme, *J. of Geophysical Res.*, **100** 16415-16430.

Meyer-Peter, E. and R. Muller, 1948: Formula for bed-load transport. *Proc. Intl Assoc. Hydr. Struct. Res. Stockholm*, 39-64.

Nikuradse, J., 1933: English translation: Law of flow in rough pipes. TM 1292, NACA, USA (in German: Gesetzmassigkeiten der turbulenten Stromung in raauhen Rohren. Forsch. Ing. Wesen. Heft 361).

Phares, D.J., Smedley, G.T. and Flagan, R.C. (2000) "The wall shear stress produced by the normal impingement of a jet on a flat surface," Journal of Fluid Mechanics, 418, pp 351-375.

Pomeroy, J.W., and Gray, D.M. (1990) Saltation of snow, Water resources research, Vol. 26(7) 1583-1594.

Pope, S.B., 2000: *Turbulent flows.* Cambridge University Press, Cambridge.

Poreh, M., Y.G. Tsuei and J.E. Cermak, 1967: Investigation of a turbulent radial wall jet. *J. appl. Mech.* June.

Rajaratnam, N. and S. Beltaos (1977) Erosion by impinging circular turbulent jets. Journal of the Hydraulic Division, ASCE, **103**:HY10 1191-1205.

Rajaratnam, N. (1982) Erosion by submerged circular jets. Journal of Hydraulics Division, ASCE, **108**:HY2 262-267.

Rajaratnam, N. and K.A. Mazurek, 2005: Impingement of circular turbulent jets on rough boundaries. *J. Hydr. Res.* **43**:6 689-695.

Shao, Y., and Lu, H., "A Simple Expression for Wind Erosion Threshold Friction Velocity, *J. Geophys. Res.,* Vol. 105 (22), 2000, pp. 437-443.

Shields, A. (1936) Anwendung der Ahnlichkeitsmechanik und der Turbulenzforschung auf die Geschiebewegung. *Mitt. Preuss. Versuchsanst. Wasserbau Schiffbau, Berlin* **26** 26 pp. [translated by W.P. Ott and J.C. van Uchelen, U.S. Dept. Agriculture, Soil Conserv. Service Coop Lab.]

Wu, S. and N. Rajaratnam, 2000: A simple method for measuring shear stress on rough boundaries. *J. Hydr. Res*. **38**:5.

Yalin, M.S. and Karahan, E., 1979: Inception of sediment transport. *ASCE J. Hydr. Div.,* **105** 1433–1443.